A&A 493, 283–290 (2009)
DOI: 10.1051/0004-6361:200810561
© ESO 2008

Astronomy & Astrophysics

Visible and near-infrared colors of Transneptunian objects and Centaurs from the second ESO large program⋆

F. E. DeMeo[1], S. Fornasier[1,2], M. A. Barucci[1], D. Perna[1,3,4], S. Protopapa[5], A. Alvarez-Candal[1], A. Delsanti[1], A. Doressoundiram[1], F. Merlin[1], and C. de Bergh[1]

[1] LESIA, Observatoire de Paris, 92195 Meudon Principal Cedex, France
e-mail: francesca.demeo@obspm.fr
[2] Université de Paris 7 Denis Diderot, Paris, France
[3] INAF – Osservatorio Astronomico di Roma, via Frascati 33, 00040 Monte Porzio Catone, Italy
[4] Università di Roma Tor Vergata, via della Ricerca Scientifica 1, 00133 Roma, Italy
[5] Max Planck Institute for Solar System Research, Lindau, Germany

Received 10 July 2008 / Accepted 9 October 2008

ABSTRACT

Aims. We investigate color properties and define or check taxonomic classifications of objects observed in our survey.
Methods. All observations were performed between October 2006 and September 2007 at the European Southern Observatory 8 m Very Large Telescope, UT1 and UT2 at the Paranal Observatory in Chile. For visible photometry, we used the FORS1 instrument, and for near-infrared, ISAAC. Taxonomic classifications from the Barucci system were assigned using G-mode analysis.
Results. We present photometric observations of 23 TNOs and Centaurs, nine of which have never been previously observed. Eighteen of these objects were assigned taxonomic classifications: six BB, four BR, two RR, and six that are given two or more categories due to insufficient data. Three objects that had been previously observed and classified, changed classes most likely due to surface variation: 26375 (1999 DE9), 28978 (Ixion), and 32532 (Thereus). Two objects, 47932 (2000 GN171) and 54598 (Bienor) had absolute magnitude values that were significantly different from previously published results, attributed to extreme lightcurve amplitudes.

Key words. techniques: photometric – Kuiper Belt – infrared: solar system

1. Introduction

By studying the colors of distant, minor bodies in our solar system, we learn about the initial conditions and evolution of the outer solar system, as well as the characteristics of the building blocks of planets. Because Transneptunian Objects (TNOs) are particularly faint and long integration times are essential for good quality data, photometry currently provides the best method of surveying a significant population of these objects. From these initial data, we can target specific objects of interest for follow-up observations. Although spectroscopy is a more useful tool for determining surface compositions, we are limited to the brightest of the TNO population to achieve acceptable signal-to-noise ratios from even the largest ground based telescopes. TNOs display a wide range of colors ranging from neutral or slightly blue to very red. The goal of surveying a large number of these objects is to identify color characteristics that relate independent populations of TNOs. A review of Transneptunian Object compositions and surface properties is provided by Barucci et al. (2008).

The first ESO (European Southern Observatory) Large Program at Paranal, Chile, which occurred between 2001 to 2003, provided excellent photometric data (Boehnhardt et al. 2002; Peixinho et al. 2004; Delsanti et al. 2006). Relevant statistical analyses were performed and all possible correlations between colors and orbital parameters were analyzed (for a complete review see Doressoundiram et al. 2008). The main result was that different colors could be identified with the cold classical objects (low inclination, red color and small size diameters), supposed to be more primitive, and the hot classical objects (with higher inclinations and diverse colors and sizes) (Doressoundiram et al. 2002).

In analyzing a significant number of objects, it is important to identify groups of objects with similar characteristics. There are two means of characterizing TNOs, according to either their dynamics or surface properties. Their dynamical orbital groups are defined by Gladman et al. (2008). Our sample includes objects from each of the following Gladman categories: resonant (objects in mean motion resonances with Neptune), detached (pericenters decoupled from Neptune), scattered (unstable orbits and high eccentricities), and classical (circular orbits and low eccentricities).

Taxonomies used to differentiate between a range of surface compositions have been used for small body populations since the 1970s (Chapman et al. 1975) when they were first applied to main belt asteroids. More advanced systems were developed for inner solar system small bodies such as the Tholen taxonomy based on 8 colors (Tholen 1984) and SMASSII (Small Main-Belt Asteroid Spectroscopic Survey II) spectral taxonomy (Bus & Binzel 2002). Classification systems are extremely useful for organizing surface characteristics, which may suggest age, composition, and surface alteration. By applying the same methods used for asteroids (multivariate statistical analysis and principal

⋆ Based on observations at the European Southern Observatory, Chile under programs 178.C-0867 and 178.C-0036.

components), the first TNO taxonomy was created using 22 objects with data for four colors ($B-V$, $V-R$, $V-I$, and $V-J$) by Barucci et al. (2001). The Barucci taxonomy is a four-class system ranging from a neutral color, BB, to intermediate red colors, BR and IR, to very red, RR.

In this paper we present the visible and near-infrared photometric results for data acquired between October 2006 and September 2007 for 23 objects, 9 of which have never been previously observed, obtained in the framework of a second ESO Large Program (PI = M.A. Barucci) devoted to observing TNOs and Centaurs with different techniques. The corresponding spectra of these objects are presented in Alvarez-Candal et al. (2008) and Guilbert et al. (2008). While we strive to observe any objects available that have never been observed photometrically, it is also important to continue to study previously observed objects and asses whether results are consistent or if there are changes occur in these objects that could reflect inhomogeneous surface properties. The visible and near-infrared observations were carried out simultaneously when possible. We calculate colors for all objects, determine taxonomic types when sufficient data are available, and verify the types for previously observed objects. Classification was performed by G-mode analysis developed in Fulchignoni et al. (2000) for the Barucci classification system (Barucci et al. 2005) using between two and five color data per object.

2. Observations

All observations were performed at the ESO 8.2 m Very Large Telescope (VLT), unit 1 (UT1) and unit 2 (UT2) at the Paranal Observatory in Chile. For visible photometry, we used the FORS1 (Focal Reducer and low dispersion Spectrograph, Appenzeller 1998) instrument located on UT2, in imaging mode with broadband Bessel *BVRI* filters (during the January 2007 visitor run), the *BVI* filters (during the September 2007 visitor run) and *VI* filters (during the service mode runs). The *BVRI* filters are centered at 0.429 μm, 0.554 μm, 0.657 μm and 0.768 μm, respectively.

Observations before April 2007 were acquired using a Tek backside thinned CCD (TK2048EB4-1) with 2048×2048 pixels, covering a $6.8' \times 6.8'$ field of view with 0.2"/pixel. The high gain mode (1.45 e^-/ADU) was used for the read out of the CCD for imaging.

Observations taken April 2007 and later were performed using two 2000×4000 E2V CCDs with a pixel size of 15 μm, and fields of view $6.8' \times 6.8'$ and $4.25' \times 4.25'$. The image scale is about 0.25"/pixel. The default setup (low gain mode) was used during the observations. The new CCDs are optimized for the blue range (shorter than 0.6 μm) and have strong fringing for wavelengths longer than 0.65 μm. Because of fringing which significantly affects the spectroscopy measurements and interpretation of features, the FORS2 instrument will be used in future observations.

For near-infrared photometry we used the instrument ISAAC (Infrared Spectrometer and Array Camera, Moorwood 1998) located at the Nasmyth B focus on UT1. Specifically, we used the short wavelength arm in imaging mode with the 1024×1024 Hawaii Rockwell array with a pixel size of 18.5 μm. The pixel scale is 0.148"/pixel and the field of view is $2.5' \times 2.5'$. The J, H, and K_s filters were used with central wavelengths of 1.25, 1.65, and 2.16 μm, respectively, each with widths of about 0.3 μm.

All observations were taken between October 2006 and September 2007 in both visitor and service modes. Total exposure times depended on the filter and each object's brightness, but were split into images with exposures less than one minute each dithered in a random pattern. The range of total exposure times in seconds for each filter ranged from B: 120–180, V: 60–90, R: 60–90, I: 120–180, J: 120–180, H: 120–720, K_s: 210–900. The airmasses of objects at the time of observation were typically below 1.3. All observations were taken under photometric sky conditions and seeing was usually equal to or less than 1 arcsec, except for the September 2007 observations when the seeing was 1.5 arcsec or less. See Table 1 for observational circumstances in which we report the orbit class of each object, date of observation as well as heliocentric and topocentric distances and phase angles.

3. Data reduction

3.1. FORS1 reduction

The CCD images were reduced and calibrated with a standard method. Master bias and flat fields from daylight calibrations were used. The instrumental magnitudes were measured using aperture photometry with an integrating radius typically about three times the average seeing, and sky subtraction was performed using an annulus width of 5–10 pixels around each object. The zero point of the telescope, extinction coefficient and color correction terms were computed for each run by a least squares fit for the standard stars. Atmospheric extinction was corrected using the standard stars and also stars in the field of the objects. The absolute calibration was obtained by the observation of several Landolt fields (Landolt 1992). After the FORS1 upgrade, significant fringing effects were noticed, which affected primarily observations in the I filter. To correct for the effects of fringing, master fringing maps were created and subtracted from the images.

3.2. ISAAC reduction

ISAAC reduction was performed with the ESO ISAAC data reduction pipeline using the Eclipse package (Devillard 1997). The recipe ghost was used to remove the electrical ghost signals created by the Hawaii detector. The "jitter" routine corrected for the odd-even column effect, an offset between odd and even columns of the array, as well as the 50 Hz pickup, which is observed as lines nearly aligned with the detector rows. The "jitter" routine was also used to subtract the master dark file and divide the master flat file, correct for bad pixels, subtract the sky level, and recombine the final images that were offset in a dither pattern. For most nights, the target flux was then measured using classical photometry methods with apertures determined by the seeing and growth curves of the objects. For data from October and November 2006, the aperture correction method was used to determine a correction factor for the full width flux using the growth curves of stars in the field. As with FORS1 data, the zero point of the telescope and extinction coefficients were computed for each night by a least squares fit for the standard stars, but color-correction terms were set to zero since they are very small. The target instrumental fluxes were then calibrated to standard magnitudes, typically UKIRT (United Kingdom Infra-Red Telescope) faint standards (Persson et al. 1998).

4. Results

We report colors and magnitudes for the 23 observed objects. Magnitudes in the V, J, H, and K_s filters are reported in Table 2.

Table 1. Observational circumstances.

Object[a]	Name	Dynamical Class[b]	Date	Δ (AU)[c]	r (AU)	α (deg)
10199	Chariklo	Centaur	20 Mar. 2007	12.496	13.276	2.7
26375	1999 DE9	Resonant(5:2)	22 Jan. 2007	34.764	35.435	1.2
28978	Ixion	Resonant(3:2)	15 Jul. 2007	41.242	42.019	0.9
32532	Thereus	Centaur	19 Sep. 2007	10.341	11.006	4.0
42355	Typhon	Scattered	24 Jan. 2007	16.710	17.542	1.8
47171	1999 TC36	Resonant(3:2)	9 Nov. 2006	30.086	30.920	1.1
47932	2000 GN171	Resonant(3:2)	23 Jan. 2007	28.373	28.352	2.0
47932	2000 GN171	Resonant(3:2)	24 Jan. 2007	28.356	28.352	2.0
47932	2000 GN171	Resonant(3:2)	24 Mar. 2007	27.519	28.346	1.1
50000	Quaoar	Classical	15 Jul. 2007	42.450	43.267	0.8
54598	Bienor	Centaur	18 Sep. 2007	17.127	18.116	0.6
55565	2002 AW197	Classical	23 Jan. 2007	45.859	46.796	0.4
55637	2002 UX25	Classical	18 Sep. 2007	41.185	42.004	0.8
60558	Echeclus	JFC	14 May 2007	11.239	12.124	2.4
83982	Crantor	Centaur	14 Jul. 2007	14.008	14.739	2.8
83982	Crantor	Centaur	16 Jul. 2007	14.032	14.741	2.9
90568	2004 GV9	Classical	13 May 2007	38.142	39.069	0.6
119951	2002 KX14	Classical	13 Jul. 2007	38.856	39.535	1.1
120132	2003 FY128	Detached	22 Jan. 2007	37.930	38.297	1.4
136199	Eris	Detached	19 Sep. 2007	95.921	96.803	0.3
136199	Eris	Detached	20 Oct. 2006	95.890	96.849	0.2
145451	2005 RM43		19 Sep. 2007	34.665	35.183	1.4
145452	2005 RN43		19 Sep. 2007	39.838	40.714	0.7
145453	2005 RR43		18 Sep. 2007	37.977	38.492	1.3
2003 AZ84		Resonant(3:2)	24 Jan. 2007	44.654	45.604	0.3
2003 QW90		Classical	9 Nov. 2006	43.516	44.227	0.9
2003 UZ117		Classical	25 Dec. 2006	38.858	39.512	1.1

[a] All objects in bold have their colors reported for the first time ever.
[b] Dynamical classes are from Gladman et al. (2008).
[c] Δ, r, and α are the topocentric and heliocentric distances and the phase angle, respectively.

In Table 2, we also provide absolute H magnitudes, labeled $H_v(1, 1, 0)$, the visible magnitude of an object if it were placed 1 AU from the sun and 1 AU from the Earth with a phase angle of zero. The equation used to calculate the absolute magnitude is expressed in Eq. (1):

$$H_v(1, 1, 0) = V(1, 1, 0) = V - 5\log(r\Delta) - \alpha\beta \quad (1)$$

where V is the visible magnitude reported in Col. 5 of Table 2, and r, Δ, and α are the heliocentric and topocentric distances and the phase angle, respectively, given in Table 1. β is the phase curve slope (mag/deg). For TNOs, we used a β value of 0.14 ± 0.03 mag/deg, the modal value of the measurements from Sheppard & Jewitt (2002). For Centaurs and Jupiter Family Comets (JFC), we used a β value of 0.11 ± 0.01 mag/deg, the result of a least squares fit by Doressoundiram et al. (2005) of the linear phase function $\phi(\alpha) = 10^{-\alpha\beta}$ of data from Bauer et al. (2003).

Mean colors with respect to the V magnitude are shown in Table 3. The errors for the colors were calculated as the square root of the sum of each magnitude error squared, $\sqrt{\mathrm{err}_1^2 + \mathrm{err}_2^2}$. When more than one observation was taken for an object, and hence more than one magnitude measurement in a certain filter existed, the weighted mean magnitude was calculated and one single color was reported. From these colors, we calculated reflectance values at each wavelength using Eq. (2):

$$R(\lambda) = 10^{-0.4[(M_F - M_V) - (M_F - M_V)_\odot]} \quad (2)$$

where (M_F) and $(M_{F\odot})$ are the magnitudes of the object and sun, respectively, at the central wavelength of filter F (specified to be $BVRIJHK_s$). The equation is normalized to unity at the central wavelength of filter V using M_V and $M_{V\odot}$, the V magnitudes of the object and sun, respectively. Solar colors listed in the first row of Table 3 are taken from Campins et al. (1985) and Hardorp (1980). In Fig. 1, a plot is shown of normalized reflectance values for all classified objects with more than three data points; a large slope variation is evident.

Some color values differ significantly from the literature, and even some previously published results disagree significantly from each other (for a summary of TNO photometry values, see Fulchignoni et al. 2008). These color differences could be attributed to inhomogeneous surface compositions or irregular shapes for objects that were not observed simultaneously in the visible and near-infrared wavelengths. Some of these objects have known lightcurves that can provide insight into the expected magnitude changes during a rotational period. These lightcurve magnitude amplitudes are listed in Table 4. A complete list of all known TNO lightcurves can be found in Sheppard et al. (2008). Objects in our sample with the most striking magnitude changes include 47932 and 54598 with magnitude changes throughout their rotational periods of 0.61 ± 0.03 and 0.75 ± 0.09, respectively.

5. Taxonomy

Barucci et al. (2005) created a new taxonomy for TNOs and Centaurs using the same method as asteroid taxonomies (Barucci et al. 1987; Tholen & Barucci 1989): principal component

Table 2. Observed magnitudes using the V, J, H, and K_s filters.

Object	Date	$t1^a$	$t2^b$	V^c	J	H	K_s	$H_v(1, 1, 0)^d$
10199	20 Mar. 2007	5:32	3:22	18.49 ± 0.05	17.00 ± 0.05	16.51 ± 0.06	16.30 ± 0.06	7.09 ± 0.05
26375	22 Jan. 2007	6:49	5:48	20.75 ± 0.04	19.22 ± 0.06	18.93 ± 0.07	18.87 ± 0.07	5.13 ± 0.05
28978	15 Jul. 2007	2:47	3:51	20.22 ± 0.05	18.63 ± 0.04	18.37 ± 0.05	18.38 ± 0.05	3.90 ± 0.06
32532	19 Sep. 2007	6:44	6:55	19.90 ± 0.03	18.55 ± 0.04	18.15 ± 0.06	18.04 ± 0.06	9.18 ± 0.03
42355	24 Jan. 2007	5:33	6:20	20.34 ± 0.02	18.78 ± 0.04	18.33 ± 0.05	18.17 ± 0.05	7.75 ± 0.04
42355	24 Jan. 2007	5:46		20.36 ± 0.02				7.77 ± 0.04
47171	09 Nov. 2006	0:58	0:58	20.25 ± 0.03	18.17 ± 0.07	17.85 ± 0.07	17.79 ± 0.08	5.25 ± 0.04
47171	09 Nov. 2006	1:09		20.26 ± 0.03				5.26 ± 0.04
47932	23 Jan. 2007	7:06	6:45	21.01 ± 0.03	19.43 ± 0.08	19.09 ± 0.09		6.20 ± 0.04
47932	23 Jan. 2007	7:15		21.04 ± 0.03				6.23 ± 0.04
47932	24 Jan. 2007	7:17	7:45	21.11 ± 0.03	19.42 ± 0.06	19.04 ± 0.07	18.98 ± 0.07	6.30 ± 0.04
47932	24 Jan. 2007	7:26		21.12 ± 0.03				6.31 ± 0.04
47932	24 Mar. 2007	5:12	5:57	21.30 ± 0.06				6.69 ± 0.07
50000	15 Jul. 2007	1:33	2:17	19.25 ± 0.05	17.07 ± 0.03	16.71 ± 0.04	16.68 ± 0.04	2.82 ± 0.06
54598	18 Sep. 2007	4:51	4:05	19.98 ± 0.03	18.46 ± 0.05	18.09 ± 0.05		7.46 ± 0.03
55565	23 Jan. 2007	5:13	5:28	20.36 ± 0.02	18.62 ± 0.05	18.28 ± 0.06	18.21 ± 0.06	3.65 ± 0.04
55565	23 Jan. 2007	5:25		20.37 ± 0.02				3.66 ± 0.04
55637	18 Sep. 2007	6:50		20.28 ± 0.06				3.98 ± 0.07
60558	14 May 2007	1:10	0:51	20.61 ± 0.06	19.13 ± 0.04	18.76 ± 0.06	18.42 ± 0.09	9.67 ± 0.06
83982	14 Jul. 2007	1:32		21.00 ± 0.07				9.12 ± 0.07
83982	16 Jul. 2007	1:03		20.91 ± 0.02				9.01 ± 0.02
90568	13 May 2007	2:44	2:14	20.20 ± 0.03	18.63 ± 0.05	18.29 ± 0.08	18.15 ± 0.05	4.25 ± 0.04
119951	13 Jul. 2007	1:29		20.95 ± 0.08				4.86 ± 0.09
120132	22 Jan. 2007	6:49	7:13	21.06 ± 0.03	19.42 ± 0.05	19.06 ± 0.06	18.95 ± 0.06	5.05 ± 0.04
120132	22 Jan. 2007	7:01		21.06 ± 0.03				5.05 ± 0.04
136199	19 Sep. 2007	5:24	9:03	18.74 ± 0.04	17.96 ± 0.04	17.88 ± 0.06	18.16 ± 0.06	-1.14 ± 0.05
136199	20 Oct. 2006	5:40	4:24	18.74 ± 0.02	17.79 ± 0.08			-1.13 ± 0.04
136199	20 Oct. 2006	5:49		18.75 ± 0.02				-1.12 ± 0.04
145451	19 Sep. 2007	9:17	9:23	20.18 ± 0.03	19.27 ± 0.06	19.07 ± 0.06	18.79 ± 0.07	4.55 ± 0.04
145452	19 Sep. 2007	4:07	3:23	20.02 ± 0.03	18.47 ± 0.05	18.16 ± 0.05	17.97 ± 0.05	3.87 ± 0.04
145452	19 Sep. 2007		4:04		18.39 ± 0.05			
145453	18 Sep. 2007	7:57	6:50	20.08 ± 0.03	19.06 ± 0.06			4.07 ± 0.04
145453	18 Sep. 2007		7:33		19.12 ± 0.06			
2003 AZ84	24 Jan. 2007	3:38	4:13	20.33 ± 0.02	19.12 ± 0.05	18.81 ± 0.05	18.75 ± 0.05	3.74 ± 0.04
2003 AZ84	24 Jan. 2007	3:47		20.33 ± 0.02				3.74 ± 0.04
2003 QW90	09 Nov. 2006	2:37	2:19	21.80 ± 0.06	19.87 ± 0.15			5.25 ± 0.07
2003 QW90	09 Nov. 2006	2:45		21.82 ± 0.06				5.27 ± 0.07
2003 UZ117	25 Dec. 2006	2:01	1:02	21.25 ± 0.04				5.16 ± 0.05
2003 UZ117	25 Dec. 2006	2:18		21.26 ± 0.04				5.17 ± 0.05

[a] UT start time for visible data.
[b] UT start time for IR data.
[c] For some objects, the visible magnitude was observed more than once in a night. Both magnitudes are reported and the observational start times are shown in Col. 3.
[d] $H_v(1, 1, 0)$ is the absolute magnitude calculated using visible magnitudes reported in this table as well as helio- and topocentric distances and the phase angle reported in Table 1. The calculation is shown as Eq. (1).

analysis (PCA) and multivariate G-mode analysis. Four groups were defined, each with capitalized two-letter designations to distinguish this TNO taxonomy notation from those for asteroids. Objects having neutral colors with respect to the Sun are classified as BB (blue objects), and those having very high slope are classified RR (very red objects). The BR group contains objects with an intermediate blue-red color, while the IR group includes moderately red objects. These classes represent objects with different surfaces. Some objects could differ in their initial compositions, which distinguish their colors, while others may have different colors and slopes because their surfaces have been affected by processes such as bombardment by energetic particles over time. Figure 1 highlights the differences between classes among our sample. It is evident that there is also wide variation in slope among the BB class objects due to the broad boundary defining the class.

Fulchignoni et al. (2000) published an extension of the G-mode analysis method, which enables the new classification of objects within the Barucci taxonomic system. Even if only a subset of the colors used in the initial taxonomy exists for an object, the algorithm provides at least a preliminary indication of its class. Objects that do not have a full set of colors for

Table 3. Mean TNO colors.

Object	Prev[a]	New[b]	Total[c]	$B-V$	$V-R$	$V-I$	$V-J$	$V-H$	$V-K_s$
Sun[d]				0.67	0.36	0.69	1.08	1.37	1.43
10199	BR	BR,BB	4		0.45 ± 0.07		1.49 ± 0.07	1.98 ± 0.08	2.19 ± 0.08
26375	IR	*	5		0.62 ± 0.02	1.12 ± 0.02	1.53 ± 0.07	1.82 ± 0.08	1.88 ± 0.08
28978	IR	BB	4		0.55 ± 0.06		1.59 ± 0.06	1.85 ± 0.07	1.84 ± 0.07
32532	BR	BB	5	0.81 ± 0.05		0.9 ± 0.13	1.35 ± 0.05	1.75 ± 0.06	1.86 ± 0.06
42355	BR	BR	5		0.48 ± 0.04	0.94 ± 0.03	1.56 ± 0.04	2.01 ± 0.05	2.17 ± 0.05
47171	RR	RR	4			1.26 ± 0.04	2.08 ± 0.08	2.4 ± 0.08	2.46 ± 0.09
47932	IR	BR,IR	5		0.59 ± 0.09	1.12 ± 0.04	1.65 ± 0.05	2.01 ± 0.06	2.13 ± 0.08
50000		RR	4		0.6 ± 0.05		2.18 ± 0.06	2.54 ± 0.06	2.57 ± 0.06
54598	BR	BR	4	0.73 ± 0.05		0.93 ± 0.16	1.52 ± 0.06	1.89 ± 0.06	
55565	IR	IR,RR	5		0.61 ± 0.03	1.16 ± 0.03	1.74 ± 0.05	2.08 ± 0.06	2.15 ± 0.06
55637	IR	RR,IR	2	1.03 ± 0.23		1.16 ± 0.34			
60558	BR	BR,BB	4		0.49 ± 0.07		1.48 ± 0.07	1.85 ± 0.08	2.19 ± 0.11
83982	RR				0.74 ± 0.09				
90568		BR	4		0.56 ± 0.03		1.57 ± 0.06	1.91 ± 0.09	2.05 ± 0.06
119951					0.61 ± 0.04				
120132		BR	5		0.59 ± 0.03	1.15 ± 0.03	1.64 ± 0.06	2 ± 0.07	2.11 ± 0.07
136199	BB	BB	5	0.85 ± 0.06		0.74 ± 0.12	0.83 ± 0.05	0.86 ± 0.07	0.58 ± 0.07
145451		BB	5	0.7 ± 0.06		0.7 ± 0.18	0.91 ± 0.06	1.11 ± 0.07	1.39 ± 0.07
145452		*	5	1.03 ± 0.07		1.13 ± 0.21	1.59 ± 0.05	1.86 ± 0.06	2.05 ± 0.06
145453		BB	3	0.71 ± 0.12		0.76 ± 0.16	0.99 ± 0.05		
2003 AZ84	BB	BB	5		0.4 ± 0.03	0.73 ± 0.03	1.21 ± 0.05	1.52 ± 0.05	1.58 ± 0.05
2003 QW90		IR,RR,BR	2			1.16 ± 0.07	1.98 ± 0.16		
2003 UZ117						0.67 ± 0.05			

[a] Previous classifications reported in Fulchignoni et al. (2008).
[b] Objects that fall within more than one class range have types listed in order of probability. Objects marked with a * did not fall within the parameters of any taxonomic class.
[c] The total number of colors used to determine the taxonomic class. Objects with more colors have a higher quality class determination.
[d] Solar Colors are taken from Hardorp (1980) and Campins et al. (1985).

classification may be assigned two taxonomic types since there is insufficient information to differentiate to which of the two classes the object belongs. We applied this algorithm to each object with more than one color data, and the resulting classes along with the colors are reported in Table 3. The objects' colors are within three sigma of their class' average values.

6. Discussion

Using between two and five color data for each object, we classified 18 of the 23 objects, and their classes are reported in Table 3. There were six BB, four BR, two RR and six designated two or more categories due to insufficient data. Three objects (83982, 119951, 2003 UZ117) had only one color and were therefore unclassifiable. Two objects (26375, 145452) did not fall within the range of the 4 taxonomic groups: objects 26375 was previously classified as IR (Fulchignoni et al. 2008), while 145452 had never been previously observed. These two objects did not fall within any particular class because their visible colors matched those of the redder IR and RR classes while their infrared colors were more consistent with the bluer BB and BR classes.

Of the nine newly observed objects, we classified six. Objects 145451 and 145453 are in class BB, 90568 and 120132 are class BR, object 50000 was classified as RR, and the sixth object, 2003 QW90 had only two colors allowing us only to exclude it from the BB class because the object is redder than BB types. Objects 119951 and 2003 UZ117 had insufficient color data to complete the analysis, while the third object 145452 had five colors but did not correspond to any of the four categories.

Fourteen objects in our sample had been previously labeled. Ten objects remained in the same class or at least one of the two designations agreed if an object had been given two types. One (83982) had only one color data and could not be classified. Three objects changed from their previous classes: 26375 (1999 DE9), 28978 (Ixion), and 32532 (Thereus).

Seven objects have known periods from their lightcurves (see Table 4 for a summary of lightcurve publications). Object 47171 is a binary Two of the objects, 47932 and 54598 (Bienor) have extreme lightcurve amplitudes (0.61 and 0.75 mag changes, see Table 4). Their calculated absolute magnitudes $H_v(1, 1, 0)$ are significantly different from previous results, but still inside the Δ magnitude value of their lightcurves. We discuss these objects and others that changed classes in further detail.

6.1. 26375 (1999 DE9)

Seven measurements combined in Fulchignoni et al. (2008) produced the previous classification (IR) of 26375. Combined with lightcurve data indicating no significant magnitude variations (see Table 4) it appears that previous measurements were robust and stable. While our visible colors agree with published results, the infrared colors with respect to V are approximately 0.3 magnitudes lower. Our $J-H$ and $J-K$ colors, however, are in good agreement with previous work (see Tables 5 and 6). Jewitt & Luu (2001) noted a feature attributed to H_2O ice (abundance around 10%), which was also detected by Barkume et al. (2008). This feature was not seen by Doressoundiram et al. (2003), suggesting that there may be heterogeneity on the surface.

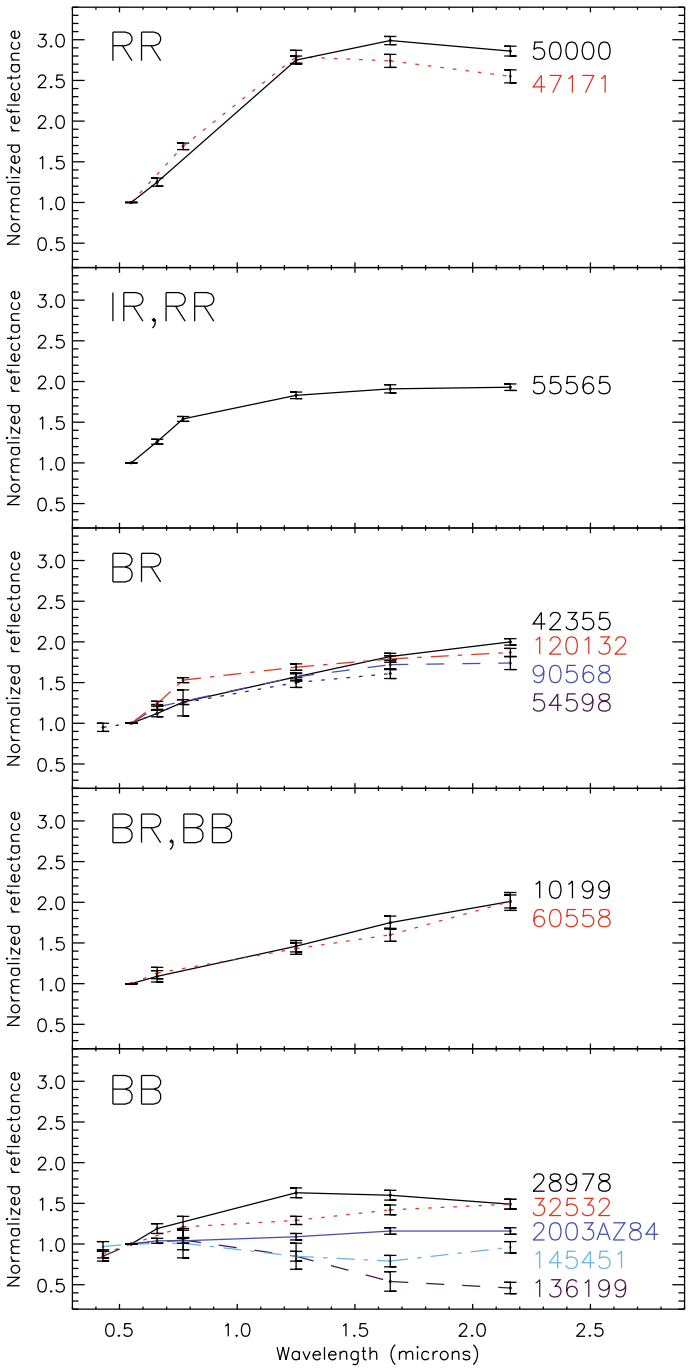


Fig. 1. Normalized Reflectance Values for 14 TNOs and Centaurs. This figure plots reflectivity values for classified objects with more than two data points. The spectra are normalized to unity at the center of the V-band (0.554 μm). Reflectivities are calculated using Eq. (2). BB objects include 28978, 32532, 136199, 145451, and 2003 AZ84. BR, BB objects are 10199 and 60558. BR objects are 42355, 54598, 90568, and 120132. The IR, RR object is 55565, and the two RR objects are 47171 and 50000.

6.2. Ixion (29878)

Ixion (28978) had been previously classified as an IR, but is a BB according to our data, which represents a significant change. The previous classification was based on one set of observations of six colors (data from Doressoundiram et al. 2007). Ixion does not have a significant lightcurve amplitude (see Table 4), although, while our $J - H$ color agrees with previous work, the

Table 4. Known lightcurve data for TNOs

Object	Δ Magnitude[a]	Period (h)[b]	Ref.[c]
26375	<0.10		1
28978	<0.05		2, 3
32532	0.16 ±0.02,0.18	4.1546 ± 0.0001(s)	4
		8.34(d)	5
42355	<0.05		2, 3
47171	<0.05		2, 3, 6
47932	0.61 ± 0.03	8.329 ± 0.005(d)	1
50000	0.13 ± 0.03	17.6788 ± 0.0004(d)	7
54598	0.75 ± 0.09	4.57 ± 0.02(s)	4
55565	0.08 ± 0.07, <0.03	8.86 ± 0.01(s)	8, 9
55637	<0.06, 0.21±0.06	7.2 or 8.4(s)	2, 10
60558	0.24 ± 0.06	13.401(s)	10
83982	0.14 ± 0.04	6.97 or 9.67(s)	3
90568	<0.08		9
120132	<0.08		9
136199	<0.01		9

[a] The peak to peak range of the lightcurve.
[b] Lightcurve periods in hours noted as single (s) or double (d) if the period has one or two maxima.
[c] Data is referenced from: 1. Sheppard & Jewitt (2002), 2. Sheppard & Jewitt (2003), 3. Ortiz et al. (2003a), 4. Ortiz et al. (2002), 5. Farnham & Davies (2003), 6. Lacerda & Luu (2006), 7. Ortiz et al. (2003b), 8. Ortiz et al. (2006), 9. Sheppard (2007), 10. Rousselot et al. (2005). For a complete listing see Sheppard et al. (2008).

Table 5. Comparison of infrared colors with previous work for selected TNOs.

Obj	$J - H$	$J - K$	Ref.[a]
26375	0.29 ± 0.09	0.35 ± 0.09	4
	0.40 ± 0.09	0.41 ± 0.13	1
	0.32 ± 0.11	0.28 ± 0.11	2
	0.29 ± 0.06	0.36 ± 0.06	3
28978	0.26 ± 0.06	0.25 ± 0.06	4
	0.30 ± 0.07	0.09 ± 0.07	1
32532	0.39 ± 0.07	0.51 ± 0.07	4
	0.34 ± 0.07	0.62 ± 0.07	1
	0.51 ± 0.04	0.62 ± 0.06	5
47932	0.37 ± 0.07	0.44 ± 0.09	4
	0.37 ± 0.11	0.54 ± 0.11	1
54598	0.36 ± 0.06		4
	0.36 ± 0.06		1
	0.35 ± 0.06		6
	0.51 ± 0.07		7

[a] References 1: Doressoundiram et al. (2007), 2: Delsanti et al. (2006), 3: Doressoundiram et al. (2003), 4: This work, 5: Barucci et al. (2002), 6: Dotto et al. (2003), 7: Delsanti et al. (2004).

$J - K$ is higher. This may correspond to surface heterogeneity. Our $V - J$ and $V - H$ colors were each almost 0.3 mag lower than seen by Doressoundiram et al. (2007), which produced a significant classification change. Slight H_2O ice features were detected in the infrared spectra by both Licandro et al. (2002) and Barkume et al. (2008).

6.3. Thereus (32532)

Thereus (32532) was previously a BR, but our data classifies it as a BB. While our optical data agree with published results, our $V - J$ value is more than 0.3 mag lower, $V - H$ is almost 0.4, and $V - K_s$ is around 0.45 mag lower than averages published by Fulchignoni et al. (2008). These differences

Table 6. Comparison of colors with previous work for selected TNOs.

Object	$B-V$	$V-R$	$V-I$	$V-J$	$V-H$	$V-K$	Ref.
26375		0.62 ± 0.02	1.12 ± 0.02	1.53 ± 0.07	1.82 ± 0.08	1.88 ± 0.08	This work
	0.97 ± 0.03	0.58 ± 0.01	1.15 ± 0.01	1.84 ± 0.04	2.17 ± 0.05	2.19 ± 0.05	Fulchignoni et al. (2008)[a]
28978		0.55 ± 0.06		1.59 ± 0.06	1.85 ± 0.07	1.84 ± 0.07	This work
	1.03 ± 0.03	0.61 ± 0.03	1.19 ± 0.04	1.88 ± 0.09	2.18 ± 0.11	1.97 ± 0.09	Doressoundiram et al. (2007)
32532	0.81 ± 0.05		0.90 ± 0.13	1.35 ± 0.05	1.75 ± 0.06	1.86 ± 0.06	This work
	0.75 ± 0.01	0.49 ± 0.02	0.94 ± 0.01	1.69 ± 0.05	2.14 ± 0.07	2.3 ± -0.05	Fulchignoni et al. (2008)
47932		0.59 ± 0.09	1.12 ± 0.04	1.65 ± 0.05	2.01 ± 0.06	2.08 ± 0.07	This work
	0.92 ± 0.01	0.62 ± 0.01	1.22 ± 0.02	1.84 ± 0.08	2.21 ± 0.14	2.38 ± 0.14	Fulchignoni et al. (2008)
	0.92 ± 0.01	0.62 ± 0.01	1.22 ± 0.02	1.84 ± 0.08	2.21 ± 0.14	2.38 ± 0.14	Fulchignoni et al. (2008)
54598	0.73 ± 0.05		0.93 ± 0.16	1.52 ± 0.06	1.89 ± 0.06		This work
	0.69 ± 0.02	0.47 ± 0.02	0.92 ± 0.05	1.74 ± 0.03	2.14 ± 0.05	2.27 ± 0.11	Fulchignoni et al. (2008)

[a] The values from Fulchignoni et al. (2008) correspond to averages of several measurements. For 26375 and 54598 it includes 7 sources each (3 and 4 for near-ir, respectively). For 32532 and 47932 there are 4 sources each (3 and 2 for near-ir, respectively).

are striking. Thereus has a double peak lightcurve of amplitude 0.18 mag (see Table 4), and has a period of over eight hours (see Table 4). Our measurements were nearly simultaneous with only an 11 min separation between visible and near-infrared data, so the difference cannot be attributed to observing different parts of the surface. Merlin et al. (2007), however, report spectral variation across the surface, which could account for differences between our data and previous work.

6.4. 47932 (2000 GN171)

For object 47932, visible and near-infrared observations were taken between 20 and 45 min apart. Although this object has a fairly long rotation period of 8.329 ± 0.005 h (see Table 4) with respect to the time difference between our visible and near-infrared observations, double maxima were detected implying that within 45 min, the object's surface shape or composition that we measured, changed significantly. It is probable that, during our exposures in J, the surface changed as well. 47932 previously classified as an IR type, by our analysis is placed in either the BR or IR classes, consistent with previous results.

We calculate an absolute magnitude $H_v(1, 1, 0)$ for 47932, ranging from 6.20 to 6.31 ± 0.04 depending on the night of observation (see Table 1). Doressoundiram et al. (2007) reports a magnitude of 6.71 ± 0.05, and McBride et al. (2003) report a similar value of 6.71 ± 0.04. The difference between our value and that reported by previous work is well within the 0.61 ± 0.03 mag lightcurve amplitude.

6.5. Bienor (54598)

Bienor (54598) has a single peak lightcurve with a period of 4.57 ± 0.02 h (see Table 4). Visible and near-infrared observations for Bienor were taken approximately 45 min apart, a time period during which the object rotated significantly. Our visible versus near-infrared observations were then acquired on different parts of the surface, which could significantly change the magnitude. The absolute magnitude $H_v(1, 1, 0)$ calculated from our results is 7.46 ± 0.03 compared to 8.04 ± 0.02 from Doressoundiram et al. (2007). This large difference in magnitude is still smaller than the lightcurve amplitude of 0.75 ± 0.09 (Table 4). A weak detection of H_2O ice features was noted by Barkume et al. (2008).

The visible colors $B-V$, $V-R$, and $V-I$, as well as the near infrared colors $J-H$ and $J-K$, are consistent with past published results. The $V-J$, $V-H$, and $V-K$ colors for several objects, however, appear to differ from the published averages (see Tables 5 and 6). Some color values are lower than in previous work, while others, such as those for Eris are higher compared to values published by Brown et al. (2005). While this difference could easily be attributed to surface heterogeneity or large lightcurve amplitudes for some objects, for objects without known variation the reason is less clear. It is important to note, however, that behavior in the optical range (such as small or large lightcurve amplitudes) may indicate but not necessarily constrain behavior in the near-infrared. The difference of colors, spans over different nights, both service and visitor mode, and several people reducing the same data independently, therefore the difference in values when compared to the literature cannot be due to weather, calibration, or reduction of a specific night. The ISAAC instrument broadband filters used for infrared observation differ from the filters that measured magnitudes for UKIRT standard stars, which we used for calibration. A color transformation between ISAAC and other systems is not yet available and could account for part of the difference, although probably not more than a few hundredths of a magnitude.

While objects that were classified in the BB class range did not change classes due to the lower infrared colors, it is important to note that the ranges of possible parameter values are far wider for BB compared with those of the BR and IR classes, implying that for equal magnitude changes an object in the BB class may not change classes, while those within the BR and IR groups may.

7. Conclusion

We report photometric observations from the ESO VLT system for 23 objects, nine of which have never been previously observed. Eighteen of these objects were given taxonomic classifications: six BB, four BR, two RR and six in two or more categories due to insufficient data.

Three objects that had been previously observed and classified, were assigned different classes: 26375 (1999 DE9), 28978 (Ixion), and 32532 (Thereus). While there is no significant lightcurve amplitude measured for 26375, H_2O ice features were noted by Jewitt & Luu (2001) and Barkume et al. (2008), but were not detected by Doressoundiram et al. (2003), suggesting that there may be heterogeneity on the surface. Ixion does not have a significant magnitude change during one rotation either, but the differences between our infrared colors and those reported by Doressoundiram et al. (2007) suggest that there is

variation over the surface. We conclude that for Thereus (32532) the change is due to surface variation reported by Merlin et al. (2007), which is also evident in its lightcurve which has significant magnitude changes (~0.16) measured by Ortiz et al. (2002).

In most of our near-infrared observations, including those of Ixion and Thereus, we report lower color values than previously published results. We measure a wide range of spectral reflectivities among the sample, which covers all four taxonomic classes. Two objects, 47932 (2000 GN171) and 54598 (Bienor), had absolute magnitude values $H_v(1, 1, 0)$ that were significantly different from previously published results. For both objects, extreme lightcurve amplitudes have been measured, which explain the variable $H_v(1, 1, 0)$ magnitude and the classification change of 47932 between different observations.

Acknowledgements. We acknowlege H. Boehnhardt for his support on photometry data analysis. F. DeMeo acknowledges funding from the Fulbright Program.

References

Alvarez-Candal, A., Fornasier, S., Barucci, M. A., de Bergh, C., & Merlin, F. 2008, A&A, 487, 741
Appenzeller, I. E. A. 1998, The Messenger, 94, 1
Barkume, K. M., Brown, M. E., & Schaller, E. L. 2008, AJ, 135, 55
Barucci, M. A., Capria, M. T., Coradini, A., & Fulchignoni, M. 1987, Icarus, 72, 304
Barucci, M. A., Fulchignoni, M., Birlan, M., et al. 2001, A&A, 371, 1150
Barucci, M. A., Boehnhardt, H., Dotto, E., et al. 2002, A&A, 392, 335
Barucci, M. A., Belskaya, I. N., Fulchignoni, M., & Birlan, M. 2005, AJ, 130, 1291
Barucci, M. A., Brown, M. E., Emery, J. P., & Merlin, F. 2008, Composition and Surface Properties of Transneptunian Objects and Centaurs, The Solar System Beyond Neptune, 143
Bauer, J. M., Meech, K. J., Fernández, Y. R., et al. 2003, Icarus, 166, 195
Boehnhardt, H., Delsanti, A., Barucci, A., et al. 2002, A&A, 395, 297
Brown, M. E., Trujillo, C. A., & Rabinowitz, D. L. 2005, ApJ, 635, L97
Bus, S. J., & Binzel, R. P. 2002, Icarus, 158, 146
Campins, H., Rieke, G. H., & Lebofsky, M. J. 1985, AJ, 90, 896
Chapman, C. R., Morrison, D., & Zellner, B. 1975, Icarus, 25, 104
Delsanti, A., Hainaut, O., Jourdeuil, E., et al. 2004, A&A, 417, 1145
Delsanti, A., Peixinho, N., Boehnhardt, H., et al. 2006, AJ, 131, 1851
Devillard, N. 1997, The Messenger, 87, 19
Doressoundiram, A., Peixinho, N., de Bergh, C., et al. 2002, AJ, 124, 2279
Doressoundiram, A., Tozzi, G. P., Barucci, M. A., et al. 2003, AJ, 125, 2721
Doressoundiram, A., Peixinho, N., Doucet, C., et al. 2005, Icarus, 174, 90
Doressoundiram, A., Peixinho, N., Moullet, A., et al. 2007, AJ, 134, 2186
Doressoundiram, A., Boehnhardt, H., Tegler, S. C., & Trujillo, C. 2008, Color Properties and Trends of the Transneptunian Objects, The Solar System Beyond Neptune, 91
Dotto, E., Barucci, M. A., & de Bergh, C. 2003, Earth Moon and Planets, 92, 157
Farnham, T. L., & Davies, J. K. 2003, Icarus, 164, 418
Fulchignoni, M., Birlan, M., & Antonietta Barucci, M. 2000, Icarus, 146, 204
Fulchignoni, M., Belskaya, I., Barucci, M. A., de Sanctis, M. C., & Doressoundiram, A. 2008, Transneptunian Object Taxonomy, The Solar System Beyond Neptune, 181
Gladman, B., Marsden, B. G., & Vanlaerhoven, C. 2008, Nomenclature in the Outer Solar System, The Solar System Beyond Neptune, 43
Guilbert, A., Alvarez-Candal, A., Merlin, F., et al. 2008, A&A, submitted
Hardorp, J. 1980, A&A, 91, 221
Jewitt, D. C., & Luu, J. X. 2001, AJ, 122, 2099
Lacerda, P., & Luu, J. 2006, AJ, 131, 2314
Landolt, A. U. 1992, AJ, 104, 340
Licandro, J., Ghinassi, F., & Testi, L. 2002, A&A, 388, L9
McBride, N., Green, S. F., Davies, J. K., et al. 2003, Icarus, 161, 501
Merlin, F., Guilbert, A., Dumas, C., et al. 2007, A&A, 466, 1185
Moorwood, A. E. A. 1998, The Messenger, 7
Ortiz, J. L., Baumont, S., Gutiérrez, P. J., & Roos-Serote, M. 2002, A&A, 388, 661
Ortiz, J. L., Gutiérrez, P. J., Casanova, V., & Sota, A. 2003a, A&A, 407, 1149
Ortiz, J. L., Gutiérrez, P. J., Sota, A., Casanova, V., & Teixeira, V. R. 2003b, A&A, 409, L13
Ortiz, J. L., Gutiérrez, P. J., Santos-Sanz, P., Casanova, V., & Sota, A. 2006, A&A, 447, 1131
Peixinho, N., Boehnhardt, H., Belskaya, I., et al. 2004, Icarus, 170, 153
Persson, S. E., Murphy, D. C., Krzeminski, W., Roth, M., & Rieke, M. J. 1998, AJ, 116, 2475
Rousselot, P., Petit, J.-M., Poulet, F., & Sergeev, A. 2005, Icarus, 176, 478
Sheppard, S. S. 2007, AJ, 134, 787
Sheppard, S. S., & Jewitt, D. C. 2002, AJ, 124, 1757
Sheppard, S. S., & Jewitt, D. C. 2003, Earth Moon and Planets, 92, 207
Sheppard, S. S., Lacerda, P., & Ortiz, J. L. 2008, Photometric Lightcurves of Transneptunian Objects and Centaurs: Rotations, Shapes, and Densities, The Solar System Beyond Neptune, 129
Tholen, D. J. 1984, Asteroid taxonomy from cluster analysis of photometry (Tucson: University of Arizona)
Tholen, D. J., & Barucci, M. A. 1989, in Asteroids II, ed. R. P. Binzel, T. Gehrels, & M. S. Matthews, 298